Pojamide: An HDAC3-Selective Ferrocene Analogue with Remarkably Enhanced Redox-Triggered Ferrocenium Activity in Cells.

Cory A. Ocasio[ʃ,‡]*, Supojjanee Sansook[†,‡], Rhiannon Jones[†], Justin M. Roberts[#], Thomas G. Scott[#], Nikolaos Tsoureas[†], Peter Coxhead[≠], Matthew Guille[≠], Graham J. Tizzard[⊥], Simon J. Coles[⊥], Helfrid Hochegger[ʃ], James E. Bradner[#] and John Spencer[†,*].

[ʃ] Genome Damage and Stability Centre, School of Life Sciences, University of Sussex, Falmer, Brighton, BN1 9RQ (UK)

[†] Department of Chemistry, School of Life Sciences, University of Sussex, Falmer, Brighton, BN1 9QJ (UK)

[#] Longwood Center (LC-2210), Dana-Farber Cancer Institute, 360 Longwood Avenue, Boston, MA 02215 (US)

[≠] School of Biological Sciences, University of Portsmouth, King Henry Building, Portsmouth, PO1 2DT (UK)

[⊥] UK National Crystallography Service, School of Chemistry, University of Southampton, Highfield Campus, Southampton, SO17 1BJ (UK)

Abstract

A ferrocene containing *ortho*-aminoanilide, *N*[1]-(2-aminophenyl)-N[8]-ferrocenyloctanediamide, **2b** (**Pojamide**) displayed nanomolar potency vs. HDAC3. Compared to **RGFP966**, a potent and selective HDAC3 inhibitor, **Pojamide** displayed superior activity in HCT116 colorectal cancer cell invasion assays; however, **TCH106** and **Romidepsin**, potent HDAC1 inhibitors, outperformed **Pojamide** in cellular proliferation and colony formation assays. Together, these data suggest that HDAC 1 & 3 inhibition is desirable to achieve maximum anti-cancer benefits. Additionally, we explored **Pojamide**-induced redox-pharmacology. Indeed, treating HCT116 cells with **Pojamide**, SNP (sodium nitroprusside) and glutathione (GSH) led to greatly enhanced cytotoxicity and DNA damage attributed to activation to an Fe(III) species.

Introduction

Histone deacetylases (HDACs) are key targets in cancer and neurodegeneration[1]. Their overexpression leads to increased deacetylated lysine/arginine levels and a condensed chromatin state resulting in transcriptional silencing. Clinically useful HDAC inhibitors (HDACis) include **SAHA**[2] (Fig. 1) and **Romidepsin**[3], which trigger growth arrest and apoptosis *via* histone hyperacetylation by pan-inhibition principally of Class I and II HDACs and other targets (*e.g.* p53).

Our increased knowledge of HDAC biology has emphasised the need for isoform-selective histone deacetylase inhibitors (HDACis)[4]. Selective inhibitors of HDAC3, (*e.g.* the benzamides **TCH106** and **RGFP966)** (Fig. 1)[5-6], are particularly attractive in CNS applications[7] and cancer[8]. However, recent studies using HDAC3-overexpressing HCT116 cells show that silencing individual HDACs (1-3) through RNAi is insufficient to achieve similar levels of growth arrest and apoptosis induced by generic HDACis such as **Trichostatin A**[9]. It is therefore likely that the inhibition of specific combinations of HDAC isoforms, HDACs 1-3 in particular, may help to achieve the full benefits of HDAC inhibition in colorectal carcinomas and possibly other cancer cells.

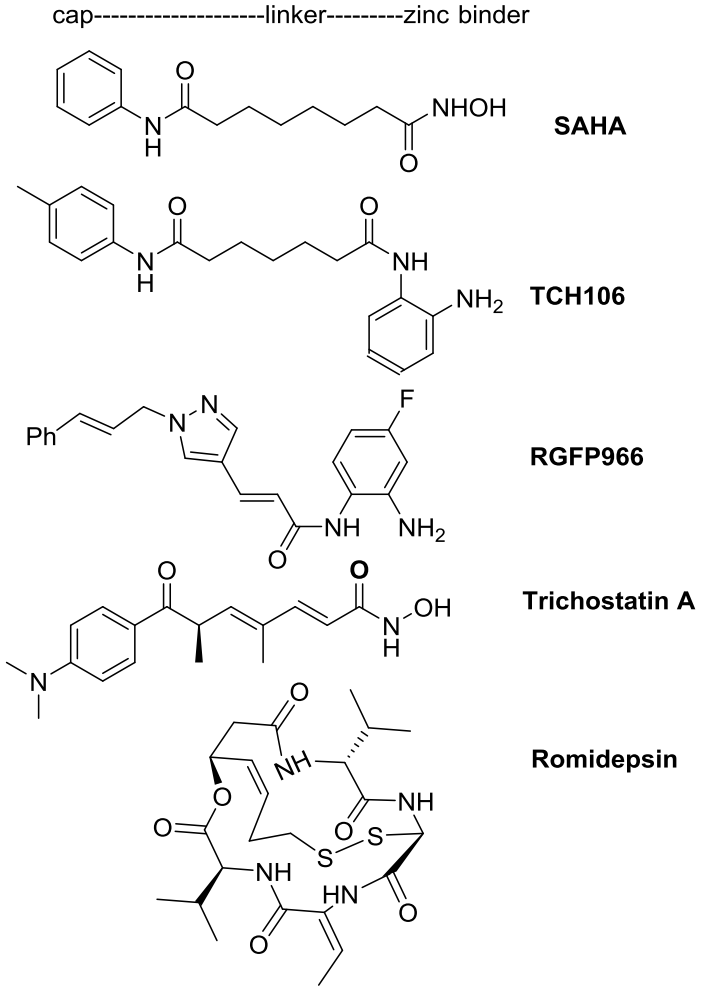

Figure 1. SAHA, and known HDACis.

Results and Discussion

Transition metal-based anticancer agents are interesting due to their novel ligand exchange and redox chemistry, the ability of a heavy metal atom to facilitate phasing in protein x-ray crystallography and the availability of geometries and oxidation states unachievable with carbon-based therapeutics[10-13]. Ferrocene-based **JAHAs** and other metal-based analogues, many containing a hydroxamic acid zinc-binding group (ZBG), are effective HDACis with good activity vs. Class I HDACs[14-25]. Guided by docking studies of a standard "cap-linker-ZBG" arrangement, we wished to extend the chemistry of **JAHAs** to *ortho*-anilide analogues, anticipating that this may lead to HDAC3-selectivity and alleviate toxicity issues documented for hydroxamate ZBGs[26].

Hence, compounds **1a** and **2a** were readily made by standard coupling reactions and were characterised in the solid state by x-ray crystallography (Figure 2)[27].

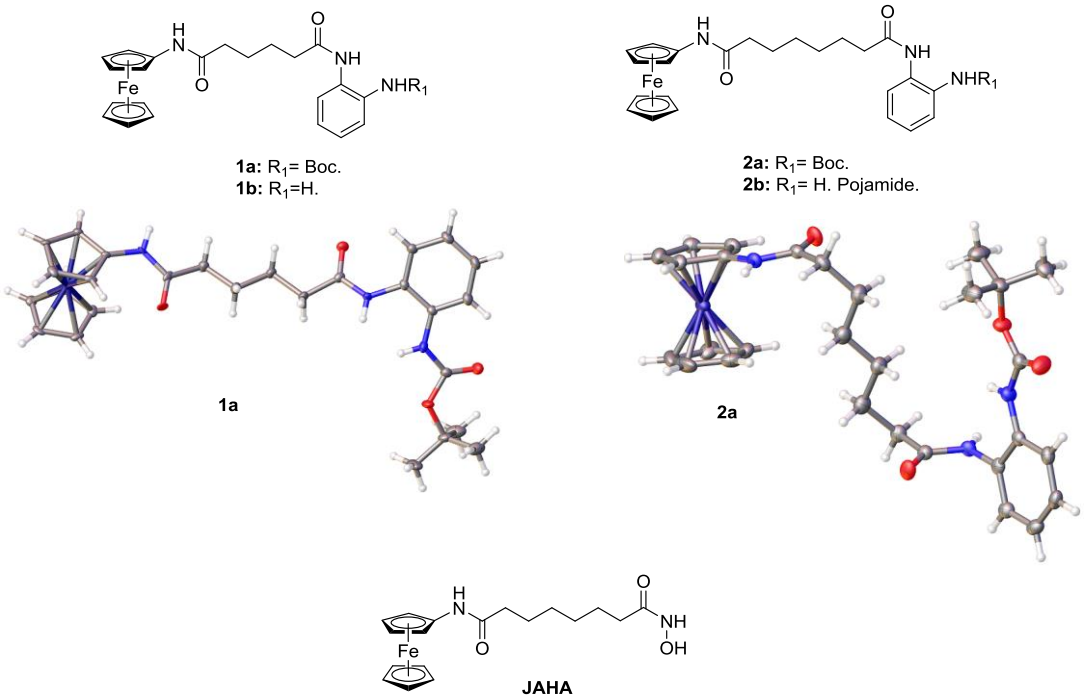

Figure 2. Ferrocene-based HDACis and precursors.

To explore the binding modes of **1b** and **2b** (**Pojamide**) in HDAC3 we performed docking studies using the structure of HDAC3 bound to co-repressor and inositol tetraphosphate (Figure 3A,B)[29]. We found that **Pojamide** bound to the zinc active site forming hydrogen bonds between the N-H of the amide and the carbonyl of Asp93, the benzamide amide N-H and the carbonyl of Gly143, the aniline NH_2 and the nitrogen of His134, and the carbonyl of Asp170 as well as the characteristic benzamide-zinc interaction.

The docked structure of **1b** is docked slightly shifted from **Pojamide**. It forms hydrogen bonds with Asp93 and Gly143. However, the substitution of the 6- carbon aliphatic chain for a 4-carbon chain results in a rotation of the benzamide group leading to a loss of key interactions, namely, hydrogen bonding with His134 and Asp170 as well as forcing zinc coordination from the benzamide aniline to the amide carbonyl (Figure 3A,B). Comparison of the active sites of HDAC3 and 8 reveals that ferrocenyl substitution for the archetypal aryl cap in HDAC inhibitors in **Pojamide** clashes with Tyr100 and Lys33 in HDAC8; assuming a similar binding mode to that of **Pojamide** in HDAC3. Thus it is assumed that ferrocenyl substitution in **Pojamide** and **1b** is responsible for HDAC3 selectivity (Figure 3C).

In addition to structural evidence supporting selective HDAC3-binding, we confirmed **Pojamide's** cell permeation and HDAC3-specificity using *Xenopus laevis* embryos (2-cell to stage 14) as a model system for

deacetylase activity. *Xenopus laevis* embryos were incubated with **1b** and **Pojamide** in order to test their bioavailability and **JAHA**, a broad HDAC inhibitor, was used as a positive control[30]. As expected **Pojamide** and **1b**, which have some selectivity towards HDAC3 (*vide infra*), did not affect □-tubulin acetylation, whereas **JAHA** increased acetylation of □-tubulin (Figure S1A). Acetylated H4K12 (H4K12ac) has, however, been shown to be a target of HDAC3 and was expected to increase if these HDAC3is were able to function in the whole organism[31]. Compound **1b** gave no sign of affecting H4K12 acetylation levels unlike **Pojamide**, which demonstrated a concentration-dependent accumulation of H4K12ac (Figure S1B). In three separate experiments the level of H4K12ac, as detected by western blotting, increased in developing embryos treated with **Pojamide**; however, embryo development was severely affected and many died (as low as 10% survival rates). For this reason, it was impossible to obtain a clear concentration-dependency for **Pojamide**, nonetheless we conclude that **Pojamide** is highly likely to be cell-permeable as an HDAC3 inhibitor, but that compound **1b** is not.

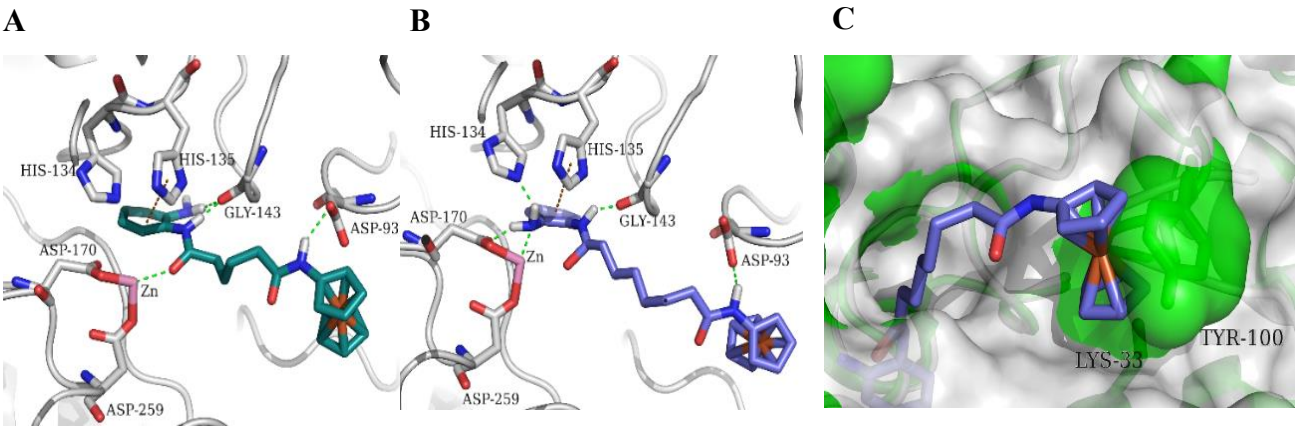

Figure 3. A,B) Docking poses of **1b** and **Pojamide** in HDAC3 (PDB code: 4A69). Top docking poses of **1b** (teal, **A**) and **Pojamide** (slate, **B**) in HDAC3. **C**) Superposition of the active sites of HDAC3 (gray) and HDAC8[28] (PDB code: 1T69, green) showing key residues overlaid with **Pojamide** top docking pose in HDAC3. Color Scheme: Hydrogen bonds shown in green dashed lines, π-π interactions shown in orange dashed lines.

Next, we tested **Pojamide** on a panel of HDACs vs. **1b**, **SAHA** and HDAC3is (Table 1)[32]. Indeed both **1b** and **Pojamide** displayed ca. 11- and 22-fold selectivity respectively towards HDAC3 over HDACs 1/2 and significantly greater selectivity over HDACs 4-8. **Pojamide**'s profile was on par with other *ortho*-anilide (benzamide) inhibitors, being most similar to that of **TCH106**, yet was outperformed by **RGFP966** with respect to HDAC3-selectivity. Only **SAHA** displayed activity vs. HDAC8 (Table 1).

With *in vitro* validation of the anti-HDAC3 activity of these ferrocene-analogues, we sought to explore their inhibitory activity in HDAC3-overexpressing cervical and colorectal cancer cell lines. HeLa, HT-29 and

HCT116 cells are tumor-forming cell lines that have been used previously as model systems to characterise HDACis[9,33-35]. We confirm in this study that compared to hTERT immortalised Retinal Pigment Epithelium (RPE) cells – cells with a longer lifespan, but incapable of forming tumors[36] – the malignant cancer cell lines HeLa, HT-29 and HCT116 all showed significantly elevated HDAC3 expression levels (Figure 4).

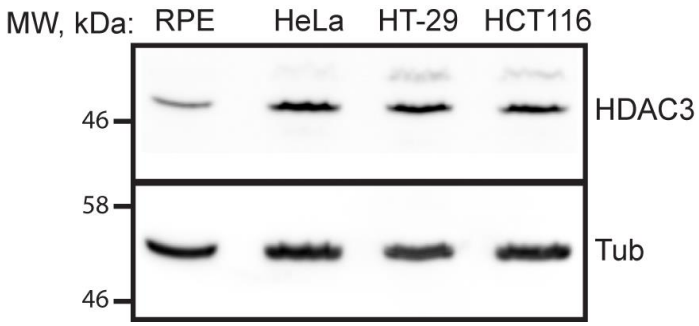

Figure 4. Western blot analysis of HDAC3 and α-Tubulin (Tub) in Retinal Pigment Epithelium (RPE), HeLa, HT-29 and HCT116 cells.

Table 1. Biochemical evaluation of HDAC isoforms 1 – 8.

	IC_{50} (μM)				
HDAC	**SAHA[a]**	**1b**	**2b[a]**	**RGFP966**	**TCH106[b]**
1	0.006 ± 0.001	8.94	1.10 ± 0.14	0.61	0.39
2	0.016 ± 0.001	13.79	1.3 ± 0.4	0.58	1.2
3	0.008 ± 0.001	0.606	0.09 ± 0.02	0.015	0.05
4	19 ± 1	>30	>30	>30	>30
5	9.7 ± 0.1	>30	>30	>30	>30
6	0.030 ± 0.001	>30	>30	>30	>30
7	>30	>30	>30	>30	>30
8	0.36 ± 0.10	>30	>30	>30	>30

[a]Profiling done in duplicate, n=8. All others n=4; [b] Slow, tight-binding inhibitor, with inverted IC_{50} and K_i values, causes IC_{50} value to drop over longer pre-incubation periods.[6] The IC_{50} value was defined as the amount of compound that caused 50% reduction in HDAC activity in comparison with DMSO-treated control and was calculated using GraphPad Prism version 6 software.

Based on these data, this small panel of cell lines was treated with increasing concentrations of **1b**, **Pojamide** and the control HDACis **RGFP966** and **TCH106**. Despite **RGFP966** showing 6.5-fold greater potency than **Pojamide** in blocking HDAC3 activity (Table 1), we found that **RGFP966** and **Pojamide** are equipotent at inhibiting HCT116 cellular proliferation, displaying GC_{50} values of 8.9 and 8.6 μM respectively (Figure 5A,

Table 2). RPE cells on the other hand were as sensitive to **Pojamide** as HCT116 cells, but were not inhibited by **RGFP966** (Figure 5B, Table 2). **TCH106** displayed superior potency against all cell lines with GC_{50} values ranging from 1 – 2 ⍰M and completely blocked colony formation at 10 ⍰M in HCT116 colony formation assays compared to 75 and 60% inhibition of colony formation by **Pojamide** and **RGFP966** respectively (Figures 5A-E, S2A-C). Interestingly, **TCH106** is 1.6- and 2.8-fold more potent toward HDAC1 inhibition than **RGFP966** and **Pojamide** respectively (Table 1) and proliferating RPE cells have been shown to overexpress HDACs 1, 2 and 5[37], suggesting that HDAC1 inhibition is in part responsible for the anti-proliferative effects of **Pojamide** and **TCH106** in these cell lines. In fact, cellular proliferation and colony formation assays using **Romidepsin**, a potent and exquisitely selective HDAC1/2 inhibitor (reported IC_{50} values of 36 and 47 nM respectively[38]), revealed a GC_{50} value of 0.52 ± 0.02 nM and near complete inhibition of colony formation at 0.5 nM; clearly the most potent anti-proliferative HDACi tested in this study (Figures 5F, S3A,B). HeLa and HT-29 cells were only mildly inhibited by **Pojamide** and **RGFP966** showing maximal growth inhibition of ~40 and 30% at 10 μM respectively, and in all cases compound **1b** was ineffective at inhibiting cellular proliferation (Figure 5A-D). This result was mirrored in *Xenopus laevis* embryo development assays, whereby **Pojamide** caused a concentration-dependent increase in acetylated H4K12 levels and **1b** did not (Figure S1).

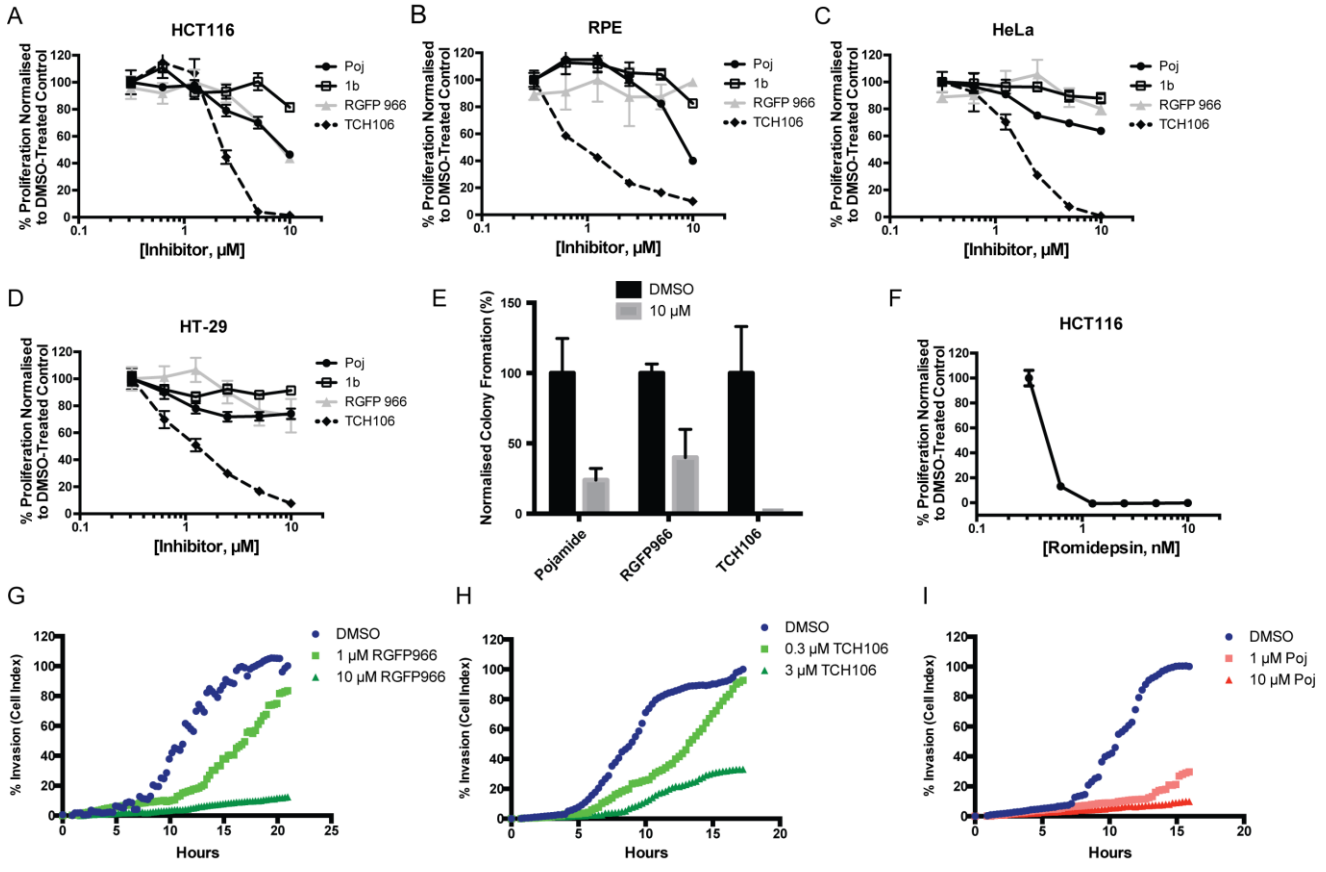

Figure 5. A-D) (**A**) HCT116, (**B**) RPE, (**C**) HeLa and (**D**) HT-29 CellTiter-Blue proliferation assays. **E**) HCT116 colony formation assays; % Colony formation (normalised to DMSO control) was quantitated manually and the average ± S.D. was plotted. **F**) Inhibitory activity of **Romidepsin** on HCT116 cellular proliferation. **G-I**) HCT116 cellular invasion assays in the presence of (**G**) **RGFP966**, (**H**) **TCH106** and (**I**) **Pojamide**.

To establish the anti-invasive properties of **Pojamide** against known HDACis, we investigated the effects of **RGFP966**, **TCH106** and **Pojamide** on HCT116 cellular invasion. In this assay, we decided to test compounds at 1x and 0.1x of their GC_{50} value determined using the HCT116 cellular proliferation assay. At the lowest concentrations tested, only **Pojamide** demonstrated robust inhibition of invasion, with about 70% inhibitory activity; however, at the 1x concentrations both **RGFP966** and **Pojamide**, exhibiting ca. 40 and 11-fold selectivity for HDAC3 inhibition respectively compared to HDAC1 (Table 1), inhibited invasion by about 90% compared to 70% for **TCH106**, which showed only 7-fold selectivity for HDAC3 vs. HDAC1 inhibition (Figure 5G-I). Based on these data and taking into consideration the activity of these compounds in the cellular proliferation assay, we conclude that HDAC isoform synergystic effects can be exploited using HDAC1- and HDAC3-selective HDACis; proliferation being attenuated more so by HDAC1, and possibly HDAC2, inhibition and invasion blocked more robustly through HDAC3 inhibition.

Table 2. Cellular characterization of HDACis

	GC_{50} (□M) or (nM)[b]				
Cell Line	**2b**	**TCH106**	**RFP966**	**Romidepsin**	**1b**
RPE	9.0 ± 0.7	≈ 1	na	nd	na
HCT116	8.6 ± 1.2	2.2 ± 0.2	8.9 ± 0.7	0.52 ± 0.02[b]	na
HeLa	na	1.5 ± 0.2	na	nd	na
HT-29	na	≈ 1	na	nd	na

[a]The GC_{50} value was defined as the amount of compound that caused 50% reduction in cellular proliferation in comparison with DMSO-treated control and was calculated using GraphPad Prism version 6 software; na = not applicable and nd = not determined.

Pojamide appears more efficacious in preventing HCT116 cellular invasion, particularly at lower concentrations (*i.e.* 1 □M). In addition, we wanted to explore the possibility that engaging a different oxidation state of the iron atom in the ferrocene moiety might offer a unique advantage at targeting cancer cells. Seminal studies with Ehrlich ascites tumor (EAT) cells and HPB (human leukemic T lymphocytes) showed that incubation with ferrocenium salts (*e.g.* $Fe(III)Cp_2PF_6$) inhibited tumor growth, whereas their ferrocene counterparts were ineffective. Indeed, ferrocenium's toxicity involves the generation of □OH radicals and the rapid induction of DNA-damage; repeated later in MCF7 and MCF10A cells[39-40].

In order to take advantage of ferrocenium cytotoxicity, we generated the ferrocenium species **3b** (**Fe(III)-Poj**) through standard means by reacting **Pojamide** with nitrosonium (NO^+) tetrafluoroborate (Scheme 1),

which was confirmed by cyclic voltammetry[41] (Figure S4). Hence, we hypothesised that intracellular generation of NO^+ in the presence of **Pojamide** might also lead to **Fe(III)-Poj** in cells.

Scheme 1. Synthetic ferrocenium Pojamides.

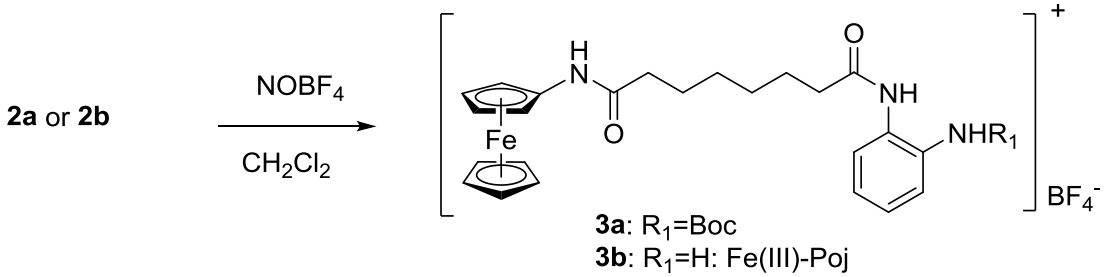

It has previously been reported that sodium nitroprusside (SNP) leads to intracellular NO^+ release[42], yet studies in neuronal PC12 cells have shown that SNP alone triggers apoptosis at concentrations greater than 30 μM[42]. To develop a cell-based assay utilising SNP as an NO^+ donor, we conducted cytotoxicity studies using the colony formation assay (Figures S5A). At 25 μM SNP, just shy of the concentration that triggers apoptosis in PC12 cells, HCT116 colony formation is reduced by about 30%; however, addition of 500 μM GSH completely eliminated SNP cytotoxicity (Figure S5A,B). GSH is a free radical scavenger, detoxifies H_2O_2 in a glutathione peroxidase-1 dependent manner[43] and its cytoprotective effects were demonstrated in our assay at concentrations of 50 and 500 μM, whereby GSH treatments, in the presence of SNP, enhanced colony formation by about 4 and 10% respectively (Figure S5A,B). The reaction of SNP with GSH to form innocuous NO may further reduce SNP cytotoxicity[44].

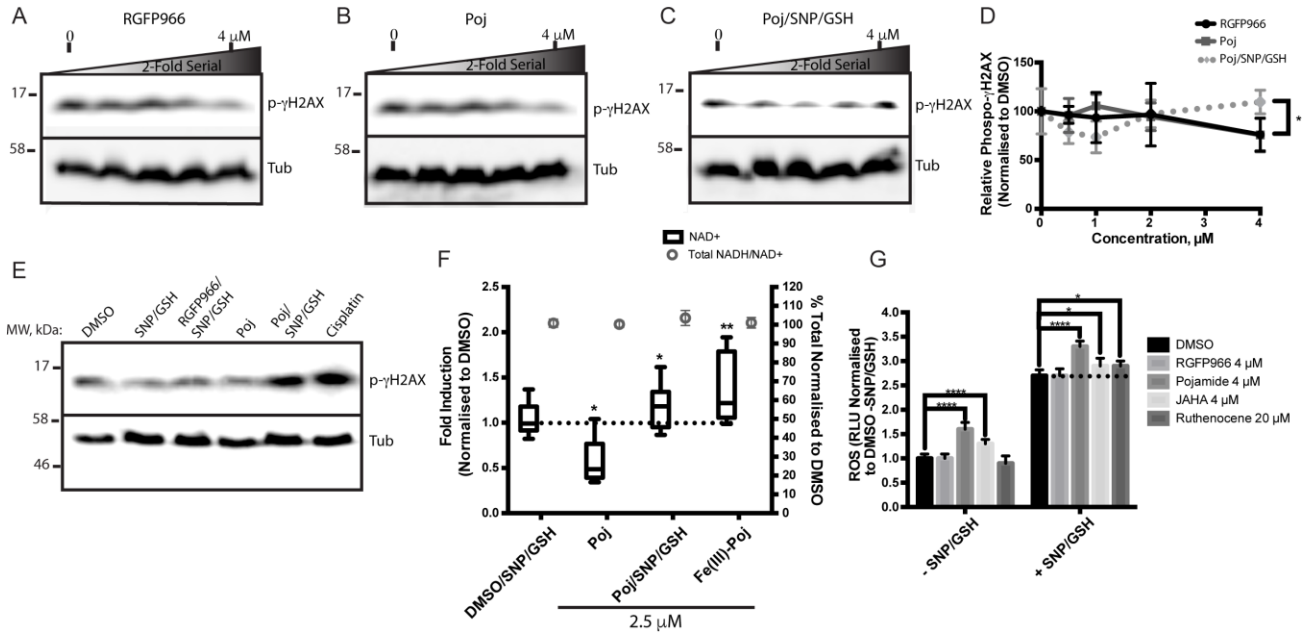

Figure 6. A-C) Western analysis of pH2AX and β-tubulin (Tub) in HCT116 cells treated for 3 d with (**A**) **RGFP966**, (**B**) **Pojamde** and (**C**) **Pojamide** + SNP/GSH. **D**) The pH2AX/Tub ratio was determined via densitometry and the average ratio normalised to DMSO control was plotted as the mean ± S.D. E) Western analysis of pH2AX and β-tubulin (Tub) in HCT116 cells treated for 6 d as indicated above. **F,G**) NAD+ fold-induction

(**F**), total NAD+/NADH (**F**) and reactive oxygen species (ROS) (**G**) levels normalised to the DMSO control; the average (n=10) was plotted ± S.D. The t-test statistical module of Prism 6.0 was used to determine p-values (ns (not statistically significant): $P > 0.05$; *: $P \leq 0.05$; **: $P \leq 0.01$; ***: $P \leq 0.001$).

After identifying the optimal conditions for SNP/GSH treatment, we treated HCT116 cells with increasing concentrations of inhibitor in the presence and absence of SNP/GSH. The generation of **Fe(III)-Poj** was monitored by blotting for the DNA-damage marker phospho-□H2AX (pH2AX)[45] (Figure 6A-D). Without SNP/GSH, increasing concentrations of **RGFP966** and **Pojamide** reduced pH2AX levels, but addition of SNP/GSH to cells treated with **Pojamide** led to an initial decrease in pH2AX, with recurrence of the DNA-damage marker at concentrations greater than 2 □M (Figure 6A-D). In a longer time-course (6 d) with 4 □M inhibitor (± SNP/GSH), only the Pojamide/SNP/GSH combination led to significant DNA-damage nearly tantamount to the levels of DNA-damage caused by cisplatin (4 □M) (Figure 6E).

To further support that our SNP/GSH treatment in the presence of **Pojamide** leads to production of **Fe(III)-Poj**, we assessed the levels of NAD+ in cells using the NAD/NADH-Glo Assay. Early studies on the one-electron transfer from NADH to ferrocenium oxidants such as $Fe(III)Cp_2PF_6$ demonstrated that ferrocenium salts can successfully oxidise NADH to NAD+ at physiologic pH in a phosphate buffer *in vitro*[46]. To recapitulate this conversion in cells, we treated HCT116 cells with DMSO/SNP/GSH and 2.5 □M Pojamide with and without SNP/GSH. For each condition, total NAD+/NADH levels remained the same, but **Pojamide** in the presence of SNP/GSH led to an increase in NAD+ levels; similar to those obtained with synthetic **Fe(III)-Poj**. In contrast, **Pojamide** treatment alone decreased NAD+ levels (Figure 6F).

In order to correlate this increase in NAD+ with oxidative stress, reactive oxygen species (ROS) levels were determined in HCT116 cells treated with **Pojamide**, the non-transition metal-based HDAC3i **RGFP966**, and other transition metal-based compounds **JAHA** and ruthenocene. Indeed, without SNP/GSH, both ferrocene-ligands **Pojamide** and **JAHA** caused an induction in ROS; an effect documented with other ferrocene-ligands such as ferrocifens and aminoferrocene prodrugs, which produce quinone methides, and in the latter case, ferrocenium catalysts for ROS production, in the absence of SNP[47,48]. DMSO, **RGFP966** and ruthenocene were assayed and showed no ROS induction without SNP/GSH. In the presence of SNP/GSH, ROS levels increased by 2.5-fold with and without **RGFP966** and, interestingly, all other conditions with SNP/GSH, **Pojamide**, **JAHA** and ruthenocene, led to greater ROS levels with **Pojamide** displaying the most significant increase, 3.3-fold, despite co-treatment with excess GSH (Figure 6G).

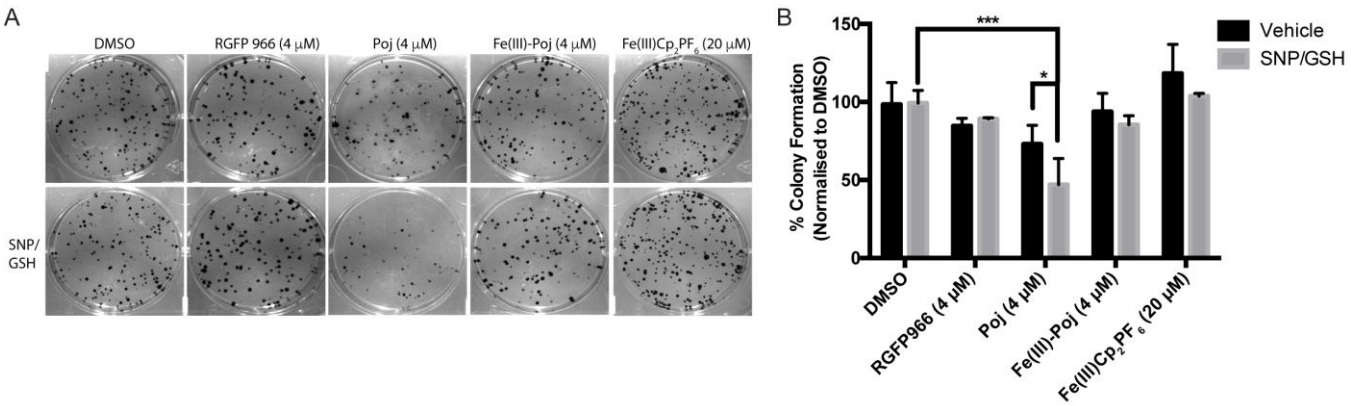

Figure 7. A) HCT116 colony formation assays; % Colony formation (**B**) (normalised to DMSO control) was quantitated manually and the average ± S.D. was plotted. The t-test statistical module of Prism 6.0 was used to determine p-values (ns (not statistically significant): P > 0.05; *: P ≤ 0.05; **: P ≤ 0.01; ***: P ≤ 0.001).

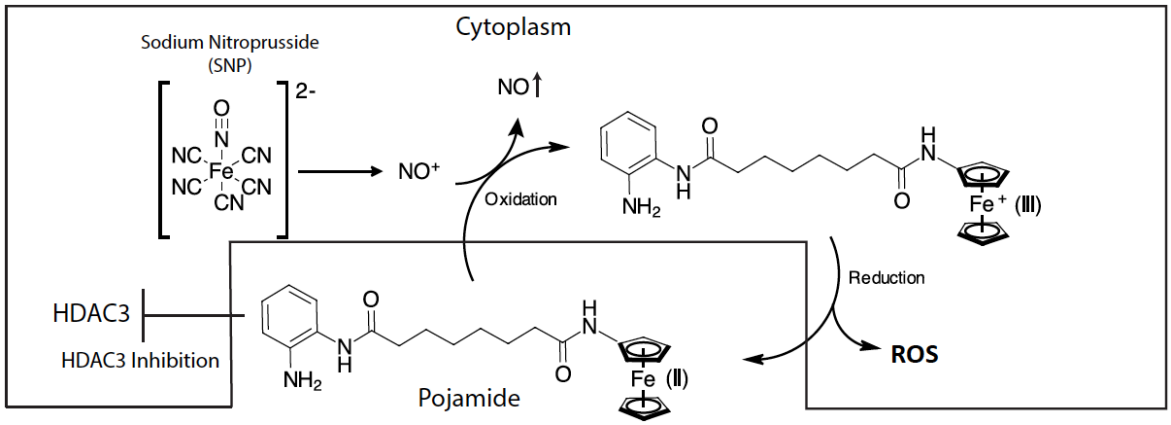

Figure 8. Model for the enhanced redox-triggered cytotoxicity of Pojamide.

With cellular validation of **Fe(III)-Poj** generation, we tested our system in the HCT116 colony formation assay (Figures 7A,B). **Pojamide** alone caused a significant decrease in colony formation, which was enhanced by addition of SNP/GSH; 27 and 53% inhibition respectively. At 4 □M, **RGFP966**, with and without SNP/GSH, displayed a 10 – 15% reduction in colony formation; however, like **Pojamide**, both ferrocenium salts were less effective without SNP/GSH. In combination with SNP/GSH, **Fe(III)-Poj** and **Fe(III)Cp_2PF_6** caused a slight, about 10%, reduction in colony formation (Figure 7A,B). Interestingly, colonies resulting from treatment with ferrocenium salts and SNP/GSH were larger, but overall fewer colonies formed; a result similar to **RGFP966** treatment. Although the cytotoxicity of ferrocenium salts is well documented, their activity is ~100-fold reduced compared to **Pojamide**[39], perhaps due to limited membrane permeability, and explains their meagre inhibitory activities at the 4 and 20 □M concentrations tested.

Conclusions

In summary, the SNP/GSH combination treatment is an ideal system for increasing the intracellular ferrocenium concentration from a **Pojamide** precursor. Also, when **Fe(III)-Poj** is reduced back to the Fe(II) species, it would be available to act upon HDACs. Due to having two separate modes of action, one which is SNP/GSH-dependent, **Pojamide** is advantageous compared to other similarly potent HDACis: its cytotoxicity is enhanced by its facile conversion to the cytotoxic Fe(III) species in cells, whilst the reduced species inhibits cellular invasion through potently targeting HDAC3 and proliferation, to a lesser extent, due to its low micromolar HDAC1 inhibitory activity (Figure 8). Lastly, co-treatments of intravenous SNP injection along with **Pojamide** administration might offer a highly efficacious strategy for managing some colon carcinomas; a strategy that might have broader, generalizable applications when used with pharmacologically distinct Fe(II)Cp_2-containing drugs (*e.g.* aminoferrocenes, ferrocifens, ferroquines).[47-50] Current studies are looking at ruthenium-based HDACis and will be reported in due course.

Experimental.

Solvents and reagents were purchased from commercial suppliers and were used without purification. Ferrocenylamine was purchased from TCI, UK, and used as such. All reactions were performed in a fume hood. NMR spectra were recorded on Varian 500 MHz or 400 MHz spectrometers and chemical shifts are reported in ppm, usually referenced to TMS as an internal standard. LCMS were performed by Shimadzu LCMS-2020 equipped with a Gemini® 5µm C18 110Å column and percentage purities were ran over 30 minutes in water/acetonitrile with 0.1% formic acid (5 min at 5%, 5%-95% over 20 min, 5 min at 95%) with the UV detector at 254 nm. High-resolution mass spectrometry (HRMS) was performed by the EPSRC National Mass Spectrometry Facility, University of Swansea. Elemental analyses were conducted by Stephen Boyer (London Metropolitan University). FT-IR were recorded on a PerkinElmer Spectrum Version 10.03.06.

***Tert*-butyl-2-(6-oxo-6-phenylamino)hexanamido)ferrocenyl carbamate 1a**.

6-Oxo-6-(ferrocenylamino)hexanoic acid[14] (493.6 mg, 1.5 mmol, 1 equiv.) and N-Boc-*o*-phenylenediamine (343.4 mg, 1.65 mmol, 1.1 equiv.) were dissolved in dichloromethane (18 mL). To this triethylamine (1.17 mL, 9 mmol) was added and the mixture was cooled in an ice bath. Next, propane phosphonic acid anhydride (T3P) (50% solution in DMF, 1.38 mL, 1.1 mmol) was added and the reaction mixture was allowed to warm up to room temperature overnight. Then the mixture was poured into a saturated solution of K_2CO_3, stirred for 30 min. and extracted into CH_2Cl_2 (DCM). The organic layer was dried ($MgSO_4$), filtered and evaporated *in vacuo*. The residue was purified by trituration with DCM to give an orange solid (576.3 mg, 74%). Crystallization by solvent evaporation of DCM provided yellow crystals. ^{1}H NMR (DMSO-d_6, 500 MHz): δ = 9.44 (1H, s, NH), 9.22 (1H, s, NH), 8.31 (1H, s, NH), 7.53 (1H, d, J=7.8 Hz, CHAr), 7.41 (1H, d, J=7.8 Hz, CHAr), 7.12-7.04 (1H, m, CHAr), 7.06 (1H, d, J=7.8 Hz, CHAr), 4.57 (2H, s, 2CH (Cp)), 4.08 (5H, s, unsusbst. Cp), 3.93 (2H, s, 2CH (Cp)), 2.37 (2H, d, J=8.3 Hz, CH_2), 2.19 (2H, t, J=6.1 Hz, CH_2), 1.65-1.56 (4H, m, $2CH_2$), 1.45 (9H, s, $3CH_3$). ^{13}C

NMR (DMSO-d_6, 126 MHz): δ = 171.0, 153.5, 130.1, 125.4, 125.3, 124.3, 124.1, 96.1, 79.8, 69.2, 64.1, 61.1, 36.2, 28.7, 28.5, 25.3.

N^1-(2-Aminophenyl)-N^6-ferrocenyladipamide 1b. The previous compound, t*ert*-butyl-2-(6-oxo-6-(phenylamino)hexanamido)ferrocenylcarbamate, (520 mg, 1.00 mmol, 1 equiv.) was suspended in dichloromethane (40 mL) and MeOH (4 mL). To this mixture 4N HCl/dioxane (8 mL) was added and the mixture was stirred at room temperature overnight. The volatiles were removed *in vacuo*, then sat. Na_2CO_3 (aq.) was added to the residue and the mixture was sonicated. The precipitate was collected by suction and washed on the frit with water, dried, triturated with CH_2Cl_2 to give the title compound as a brown solid (318 mg, 76%). ^{1}H NMR (DMSO-d_6): 9.21 (1H, s, NH), 9.09 (1H, s, NH), 7.15 (1H, d, J=7.8 Hz, CHAr), 6.78-6.73 (1H, m, CHAr), 6.70 (1H, dd, J=7.8, 1.4 Hz, CHAr), 6.53 (1H, dd, J=7.8, 1.4 Hz, CHAr), 4.80 (2H, s, NH_2), 4.56 (2H, s, 2CH (Cp)), 4.08 (5H, s, unsubst. Cp), 3.92 (2H, s, 2CH (Cp)), 2.36-2.32 (2H, m, CH_2), 2.25-2.10 (2H, m, CH_2), 1.68-1.54 (4H, m, $2CH_2$). ^{13}C NMR (DMSO-d_6, 126 MHz): δ = 171.4, 171.1, 142.3, 126.1, 125.7, 124.1, 116.6, 116.3, 96.1, 69.2, 64.1, 61.1, 36.3, 36.1, 25.5. HRMS-ESI (m/z): found 420.1366, calc. for $[C_{22}H_{26}FeN_3O_2]^+$ 420.1369. Anal. calcd (%) for $C_{22}H_{25}FeN_3O_2$: C, 63.02; H, 6.01; N, 10.02. Found (%): C, 62.85; H, 6.05; N, 9.84.

Tert-butyl-2-(8-oxo-8-(phenylamino)octanamido) ferrocenylcarbamate 2a. Methyl-8-oxo-8-(ferrocenylamino)octanoic acid (215 mg, 0.6 mmol, 1 equiv.) and N-Boc-*o*-phenylenediamine (137.4 mg, 0.66 mmol, 1.1 equiv.) were dissolved in dichloromethane (7.7 mL). To this triethylamine (0.5 mL, 3.6 mmol) was added and the mixture was cooled in an ice bath. Next, propane phosphonic acid anhydride T3P (50% solution in DMF, 0.59 mL, 0.66 mmol) was added and the reaction mixture was allowed to warm up to room temperature overnight. Then the mixture was poured into saturated solution of K_2CO_3, stirred for 30 min. and extracted into CH_2Cl_2. The organic layer was dried ($MgSO_4$), filtered and evaporated *in vacuo*. The residue was purified by trituration with DCM to give the orange solid (233.1 mg, 71%). Crystallization by solvent evaporation of DCM provided yellow crystals. ^{1}H NMR (DMSO-d_6): 9.40 (1H, s, NH), 9.15 (1H, s, NH), 8.26 (1H, s, NH), 7.54-7.48 (1H, m, CHAr), 7.42-7.35 (1H, m, CHAr), 7.13-7.09 (1H, m, CHAr), 7.08-7.03 (1H, m, CHAr), 4.55 (2H, s, 2CH (Cp)), 4.06 (5H, s, unsusbt. Cp), 3.91 (2H, s, 2CH (Cp)), 2.33 (2H, t, J=7.4 Hz, CH_2), 2.14 (2H, t, J=7.4 Hz, CH_2), 1.62-1.54 (4H, m, $2CH_2$), 1.44 (9H, s, $3CH_3$), 1.38-1.26 (4H, m, 2CH2). ^{13}C NMR (DMSO-d_6, 126 MHz): δ = 171.6, 171.2, 142.3, 126.1, 125.7, 124.1, 116.6, 116.3, 96.1, 69.1, 64.1, 61.0, 39.7, 39.5, 36.4, 36.2, 29.0, 28.9, 25.7, 25.6.

N^1-(2-Aminophenyl)-N^8-ferrocenyloctanediamide 2b (Pojamide)

Tert-butyl-2-(8-oxo-8-(phenylamino)octanamido)ferrocenyl carbamate (136.8 mg, 0.25 mmol, 1 equiv.) was suspended in dichloromethane (10 mL) and MeOH (1 mL). To this mixture 4N HCl/dioxane (2 mL) was added and the mixture was stirred at room temperature overnight. The volatiles were removed *in vacuo*, then sat. Na_2CO_3 (aq.) was added to the residue and the mixture was sonicated. The precipitate was collected

by suction and washed on the frit with water, dried, triturated with CH_2Cl_2 to give the title compound as a brown solid (82 mg, 73%). ^{1}H NMR (DMSO-d_6): 9.18 (1H, s, NH), 9.05 (1H, s, NH), 7.14 (1H, dd, J=8.0, 1.5 Hz, CHAr), 6.91-6.84 (1H, m, CHAr), 6.70 (1H, dd, J=8.0, 1.5 Hz, CHAr), 6.54-6.48 (1H, m, CHAr), 4.78 (2H, s, NH_2), 4.57 (2H, t, J=1.9 Hz, 2CH (Cp)), 4.08 (5H, s, unsubst. Cp), 3.92 (2H, t, J=1.9 Hz, 2CH (Cp)), 2.31 (2H, t, J=7.4 Hz, CH_2), 2.15 (2H, t, J=7.4 Hz, CH_2), 1.68-1.53 (4H, m, $2CH_2$), 1.35-1.29 (4H, m, $2CH_2$). ^{13}C NMR (DMSO-d_6, 126 MHz): δ = 171.6, 171.2, 142.3, 126.1, 125.7, 124.1, 116.6, 116.3, 96.1, 69.1, 64.1, 61.0, 39.7, 39.5, 36.4, 36.2, 29.0, 28.9, 25.7, 25.6. HRMS-ESI (m/z): found 448.1675, calc. for $[C_{24}H_{30}FeN_3O_2]^+$ 448.1682. Anal. Calcd (%) for $C_{24}H_{29}FeN_3O_2$: C, 64.44; H, 6.53; N, 9.39. Found (%): C, 64.23; H, 6.60; N, 9.29.

Tert-butyl-2-(8-oxo-8-(phenylamino)octanamido) ferroceniumcarbamate tetrafluoroborate, 3a. *Tert*-butyl-2-(8-oxo-8-(phenylamino)octanamido)ferrocenylcarbamate (109.5 mg, 0.2 mmol, 1 equiv.) was suspended in dry DCM (5 mL). To this $NOBF_4$ (37.4 mg, 0.32 mmol, 1.6 equiv.) was added. The color of the solution changed from yellow to dark brown. Filtration afforded the title compound as a dark brown solid (89 mg, 70%). ^{19}F NMR (DMSO-d_6): -29.53. ^{11}B NMR (DMSO-d_6): -2.56. $C_{29}H_{37}BF_4FeN_3O_4$: C, 54.92; H, 5.88; N, 6.62. Found (%): C, 55.08; H, 5.84; N, 6.57. FTIR (cm^{-1}): 992 (BF_4^-).

N^1-(2-Aminophenyl)-N^8-ferroceniumoctanediamide tetrafluoroborate, 3b (Fe(III)-Poj). N^1-(2-Amino-phenyl)-N^8-ferrocenyloctanediamide (100 mg, 0.2 mmol, 1 equiv.) was suspended in dry DCM (5 mL). To this $NOBF_4$ (37.4 mg, 0.32 mmol, 1.6 equiv.) was added. The color of the solution changed from yellow to dark brown. Filtration afforded the title compound as a dark brown solid (78 mg, 73%). ^{19}F NMR (DMSO-d_6): -29.53. ^{11}B NMR (DMSO-d_6): -1.34. $C_{24}H_{29}BF_4FeN_3O_2$: C, 67.12; H, 5.80; N, 9.49. Found (%): C, 66.97; H, 5.84; N, 9.31. FTIR (cm^{-1}): 1038 (BF_4).

AUTHOR INFORMATION

Corresponding Authors

* Cory A. Ocasio; co211@sussex.ac.uk; +44 (0)1273 678976

* John Spencer; J.Spencer@sussex.ac.uk; +44 (0)1273 877374

Author Contributions

All authors have given approval to the final version of the manuscript. ‡These authors contributed equally.

AUTHOR INFORMATION.

The authors declare no competing financial interests.

ACKNOWLEDGMENT

We thank the Thai Royal Government for support (SS), the European Community's Seventh Framework Programme [FP7/2007-2013] under grant agreement no: PIIF-GA-2011-301062 (CAO), the CRUK grant C28206/A14499 (HH) and the EPSRC UK National Mass Spectrometry Facility at Swansea University.

REFERENCES

1. Khan, O.; La Thangue, N. B., HDAC inhibitors in cancer biology: emerging mechanisms and clinical applications. *Immunol Cell Biol* **2012,** *90* (1), 85-94.
2. Marks, P. A.; Breslow, R., Dimethyl sulfoxide to vorinostat: development of this histone deacetylase inhibitor as an anticancer drug. *Nat Biotechnol* **2007,** *25* (1), 84-90.
3. Mizutani, H.; Hiraku, Y.; Tada-Oikawa, S.; Murata, M.; Ikemura, K.; Iwamoto, T.; Kagawa, Y.; Okuda, M.; Kawanishi, S., Romidepsin (FK228), a potent histone deacetylase inhibitor, induces apoptosis through the generation of hydrogen peroxide. *Cancer Sci* **2010,** *101* (10), 2214-9.
4. Thaler, F.; Mercurio, C., Towards selective inhibition of histone deacetylase isoforms: what has been achieved, where we are and what will be next. *ChemMedChem* **2014,** *9* (3), 523-6.
5. Malvaez, M.; McQuown, S. C.; Rogge, G. A.; Astarabadi, M.; Jacques, V.; Carreiro, S.; Rusche, J. R.; Wood, M. A., HDAC3-selective inhibitor enhances extinction of cocaine-seeking behavior in a persistent manner. *Proc Natl Acad Sci U S A* **2013,** *110* (7), 2647-52.
6. Rai, M.; Soragni, E.; Chou, C. J.; Barnes, G.; Jones, S.; Rusche, J. R.; Gottesfeld, J. M.; Pandolfo, M., Two new pimelic diphenylamide HDAC inhibitors induce sustained frataxin upregulation in cells from Friedreich's ataxia patients and in a mouse model. *PLoS One* **2010,** *5* (1), e8825.
7. Weïwer, M.; Lewis, M. C.; Wagner, F. F.; Holson, E. B., Therapeutic potential of isoform selective HDAC inhibitors for the treatment of schizophrenia. *Future Medicinal Chemistry* **2013,** *5* (13), 1491–1508.
8. Marson, C. M.; Matthews, C. J.; Atkinson, S. J.; Lamadema, N.; Thomas, N. S., Potent and Selective Inhibitors of Histone Deacetylase-3 Containing Chiral Oxazoline Capping Groups and a N-(2-Aminophenyl)-benzamide Binding Unit. *J Med Chem* **2015,** *58* (17), 6803-18.
9. Wilson, A. J.; Byun, D.-S.; Popova, N.; Murray, L. B.; L'Italien, K.; Sowa, Y.; Arango, D.; Velcich, A.; Augenlicht, L. H.; Mariadason, J. M., Histone Deacetylase 3 (HDAC3) and Other Class I HDACs Regulate Colon Cell Maturation and p21 Expression and Are Deregulated in Human Colon Cancer. *Journal of Biological Chemistry* **2006,** *281* (19), 13548 - 13558.
10. Meggers, E., Exploring biologically relevant chemical space with metal complexes. *Curr Opin Chem Biol* **2007,** *11* (3), 287-92.
11. Meggers, E., Targeting proteins with metal complexes. *Chem Commun (Camb)* **2009,** (9), 1001-10.
12. Kilpin, K. J.; Dyson, P. J., Enzyme inhibition by metal complexes: concepts, strategies and applications. *Chemical Science* **2013,** *4* (4), 1410.

13. Gasser, G.; Ott, I.; Metzler-Nolte, N., Organometallic Anticancer Compounds. *J Med Chem* **2011**, *54*, 3–25.
14. Spencer, J.; Amin, J.; Wang, M.; Packham, G.; Alwi, S. S.; Tizzard, G. J.; Coles, S. J.; Paranal, R. M.; Bradner, J. E.; Heightman, T. D., Synthesis and Biological Evaluation of JAHAs: Ferrocene-Based Histone Deacetylase Inhibitors. *ACS Med Chem Lett* **2011,** *2* (5), 358-362.
15. Spencer, J.; Amin, J.; Boddiboyena, R.; Packham, G.; Cavell, B. E.; Syed Alwi, S. S.; Paranal, R. M.; Heightman, T. D.; Wang, M.; Marsden, B.; Coxhead, P.; Guille, M.; Tizzard, G. J.; Coles, S. J.; Bradner, J. E., Click JAHAs: conformationally restricted ferrocene-based histone deacetylase inhibitors. *MedChemComm* **2012,** *3* (1), 61.
16. Leonidova, A.; Mari, C.; Aebersold, C.; Gasser, G., Selective Photorelease of an Organometallic-Containing Enzyme Inhibitor. *Organometallics* **2016,** *35* (6), 851-854.
17. Cross, J. M.; Blower, T. R.; Gallagher, N.; Gill, J. H.; Rockley, K. L.; Walton, J. W., Anticancer RuII and RhIII Piano-Stool Complexes that are Histone Deacetylase Inhibitors. *ChemPlusChem* **2016,** *81*, 1276 – 1280.
18. Cázares-Marinero, J. d. J.; Buriez, O.; Labbé, E.; Top, S.; Amatore, C.; Jaouen, G., Synthesis, Characterization, and Antiproliferative Activities of Novel Ferrocenophanic Suberamides against Human Triple-Negative MDA-MB-231 and Hormone-Dependent MCF-7 Breast Cancer Cells. *Organometallics* **2013,** *32* (20), 5926-5934.
19. Ye, R. R.; Tan, C. P.; He, L.; Chen, M. H.; Ji, L. N.; Mao, Z. W., Cyclometalated Ir(III) complexes as targeted theranostic anticancer therapeutics: combining HDAC inhibition with photodynamic therapy. *Chem Commun (Camb)* **2014,** *50* (75), 10945-8.
20. Ye, R. R.; Ke, Z. F.; Tan, C. P.; He, L.; Ji, L. N.; Mao, Z. W., Histone-deacetylase-targeted fluorescent ruthenium(II) polypyridyl complexes as potent anticancer agents. *Chemistry* **2013,** *19* (31), 10160-9.
21. Librizzi, M.; Longo, A.; Chiarelli, R.; Amin, J.; Spencer, J.; Luparello, C., Cytotoxic Effects of Jay Amin Hydroxamic Acid (JAHA), a Ferrocene-Based Class I Histone Deacetylase Inhibitor, on Triple-Negative MDA-MB231 Breast Cancer Cells. *Chemical Research in Toxicology* **2012,** *25* (11), 2608-2616.
22. Librizzi, M.; Spencer, J.; Luparello, C., Biological Effect of a Hybrid Anticancer Agent Based on Kinase and Histone Deacetylase Inhibitors on Triple-Negative (MDA-MB231) Breast Cancer Cells. *Int J Mol Sci* **2016,** *17* (8), 1235.
23. Griffith, D.; Morgan, M. P.; Marmion, C. J., A novel anti-cancer bifunctional platinum drug candidate with dual DNA binding and histone deacetylase inhibitory activity. *Chem Commun* **2009,** (44), 6735-7.
24. Cana, D.; Dongo, H. W. P. N.; Spingler, B.; Schmutz, P.; Raposinho, P.; Santos, I.; Alberto, R., The [(Cp)M(CO)3] (M¼Re, 99mTc) Building Block for Imaging Agents and Bioinorganic Probes: Perspectives and Limitations. *Chemistry and Biodiversity* **2012,** *9*, 1849-1866.

25. Chow, K. H.; Sun, R. W.; Lam, J. B.; Li, C. K.; Xu, A.; Ma, D. L.; Abagyan, R.; Wang, Y.; Che, C. M., A gold(III) porphyrin complex with antitumor properties targets the Wnt/beta-catenin pathway. *Cancer Res* **2010,** *70* (1), 329-37.
26. Shen, S.; Kozikowski, A. P., Why Hydroxamates May Not Be the Best Histone Deacetylase Inhibitors--What Some May Have Forgotten or Would Rather Forget? *ChemMedChem* **2016,** *11* (1), 15-21.
27. Coles, S. J.; Gale, P. A., Changing and challenging times for service crystallography. *Chem. Sci.* **2012,** *3* (3), 683-689.
28. Somoza, J. R.; Skene, R. J.; Katz, B. A.; Mol, C.; Ho, J. D.; Jennings, A. J.; Luong, C.; Arvai, A.; Buggy, J. J.; Chi, E.; Tang, J.; Sang, B. C.; Verner, E.; Wynands, R.; Leahy, E. M.; Dougan, D. R.; Snell, G.; Navre, M.; Knuth, M. W.; Swanson, R. V.; McRee, D. E.; Tari, L. W., Structural snapshots of human HDAC8 provide insights into the class I histone deacetylases. *Structure* **2004,** *12* (7), 1325-1334.
29. Watson, P. J.; Fairall, L.; Santos, G. M.; Schwabe, J. W. R., Structure of Hdac3 Bound to Co-Repressor and Inositol Tetraphosphate. *Nature* **2012,** *481* (7381), 335-340.
30. Spencer, J.; Amin, J.; Callear, S.; Tizzard, G.; Coles, S.; Coxhead, P.; Guille, M., Synthesis and evaluation of metallocene containing methylidene-1,3-dihydro-2H-indol-2-ones as kinase inhibitors. *Metallomics* **2011,** *3* (6), 600-608.
31. Jiang, Y.; Hsieh, J., HDAC3 controls gap 2/mitosis progression in adult neural stem/progenitor cells by regulating CDK1 levels. *Proc Natl Acad Sci U S A.* **2014,** *111* (37), 13541-6.
32. Bradner, J.; West, N.; Grachan, M.; Greenberg, E.; Haggarty, S.; Warnow, T.; Mazitschek, R., Chemical phylogenetics of histone deacetylases. *Nat Chem Biol* **2010,** *6* (3), 238-243.
33. Mariadason, J. M., HDACs and HDAC inhibitors in colon cancer. *Epigenetics* **2008,** *3* (1), 28 - 37.
34. Spurling, C. C.; Godman, C. A.; Noonan, E. J.; Rasmussen, T. P.; Rosenberg, D. W.; Giardina, C., HDAC3 Overexpression and Colon Cancer Cell Proliferation and Differentiation. *Molecular Carcinogenesis* **2008,** *47*, 137 - 147.
35. Alcarraz-Vizán, G.; Boren, J.; Lee, W.-N. P.; Cascante, M., Histone deacetylase inhibition results in a common metabolic profile associated with HT29 differentiation. *Metabolomics* **2010,** *6*, 229 - 237.
36. ATCC, 1992.
37. Xiao, W.; Chen, X.; Liu, X.; Luo, L.; Ye, S.; Liu, Y., Trichostatin A, a histone deacetylase inhibitor, suppresses proliferation and epithelial-mesenchymal transition in retinal pigment epithelium cells. *J. Cell. Mol. Med.* **2014,** *18* (4), 646 - 655.
38. Furumai, R.; Matsuyama, A.; Kobashi, N.; Lee, K. H.; Nishiyama, M.; Nakajima, H.; Tanaka, A.; Komatsu, Y.; Nishino, N.; Yoshida, M.; Horinouchi, S., FK228 (depsipeptide) as a natural prodrug that inhibits class I histone deacetylases. *Cancer Res.* **2002,** *62* (17), 4916-4921.
39. Osella, D.; Ferrali, M.; Zanello, P.; Laschi, F.; Fontani, M.; Nervi, C.; Cavigiolio, G., On the mechanism of the antitumor activity of ferrocenium derivatives. *Inorganica Chimica Acta* **2000,** *306*, 42-48.

40. Acevedo-Morantes, C. Y.; Meléndez, E.; Singh, S. P.; Ramírez-Vick, J. E., Cytotoxicity and Reactive Oxygen Species Generated by Ferrocenium and Ferrocene on MCF7 and MCF10A Cell Lines. *Cancer Science & Therapy* **2012,** *4* (9), 271-275.
41. Chung, J.-Y.; Schulz, C.; Bauer, H.; Sun, Y.; Sitzmann, H.; Auerbach, H.; Pierik, A. J.; Schünemann, V.; Neuba, A.; Thiel, W. R., Cyclopentadienide Ligand CpC− Possessing Intrinsic Helical Chirality and Its Ferrocene Analogues. *Organometallics* **2015,** *34*, 5374-5382.
42. Kayahara, M.; Felderhoff, U.; Pocock, J.; Hughes, M. N.; Mehmet, H., Nitric oxide (NO.) and the nitrosonium cation (NO+) reduce mitochondrial membrane potential and trigger apoptosis in neuronal PC12 cells. *Biochemical Society Transactions* **1998,** *26*, 42.
43. Quintana-Cabrera, R.; Bolaños, J. P., Glutathione and γ-glutamylcysteine in hydrogen peroxide detoxification. *Methods Enzymol.* **2013,** *527*, 129 - 144.
44. Grossi, L.; D'Angelo, S., Sodium Nitroprusside: Mechanism of NO Release Mediated by Sulfhydryl-Containing Molecules. *Journal of Medicinal Chemistry* **2005,** *48*, 2622-2626.
45. Sharma, A.; Singh, K.; Almasan, A., Histone H2AX phosphorylation: a marker for DNA damage. *Methods Mol. Biol.* **2012,** *920*, 613-626.
46. Carlson, B. W.; Miller, L. L., Oxidation of NADH by Ferrocenium Salts. Rate-Limiting One-Electron Transfer. *J Am Chem Soc* **1983,** *105*, 7454-7456.
47. Jaouen, G.; Vessieres, A.; Top, S., Ferrocifen type anti cancer drugs. *Chem Soc Rev* **2015,** *44* (24), 8802-8817.
48. Hagen, H.; Marzenell, P.; Jentzsch, E.; Wenz, F.; Veldwijk, M. R.; Mokhir, A., Aminoferrocene-based prodrugs activated by reactive oxygen species. *J Med Chem* **2012,** *55* (2), 924-934.
49. Leonidova, A.; Anstaett, P.; Pierroz, V.; Mari, C.; Spingler, B.; Ferrari, S.; Gasser, G., Induction of Cytotoxicity through Photorelease of Aminoferrocene. *Inorg Chem* **2015,** *54* (20), 9740-9748.
50. Dive, D.; Biot, C., Ferrocene conjugates of chloroquine and other antimalarials: the development of ferroquine, a new antimalarial. *ChemMedChem* **2008,** *3* (3), 383-391.